Electron-nuclear double-resonance study of NaF:Fe^+ associated with a Na^+ vacancy

Nak Sam Chung,* S. Lewis Meyer,† and Robert Lee Mieher
Department of Physics, Purdue University, West Lafayette, Indiana 47907
(Received 30 May 1978)

An electron-nuclear double-resonance (ENDOR) study of a paramagnetic Fe^+ center in an orthorhombic site in NaF (the orthorhombic center) is reported. The hyperfine constants of the orthorhombic center have been determined for the fluorine-lattice nuclei in the first two fluorine shells, where each shell has three inequivalent sets of equivalent nuclei due to the presence of a vacancy. These results are consistent with the model of Fe^+ ions substitutionally occupying the Na^+ sites and associated with a nearest Na^+ vacancy (1,1,0). The ENDOR results show that the vacancy is located along the axis associated with the g value of 4.588.

I. INTRODUCTION

When transition-metal ions are incorporated in alkali-halide crystals, they are usually located substitutionally on a cation site with a divalent charge state, and it is necessary to compensate the additional positive charge.[1-5] Watkins has performed a detailed electron-paramagnetic-resonance (EPR) investigation of Mn^{2+} in LiCl, NaCl, and KCl.[2] Hall *et al.* have made extensive EPR measurements of iron-group ions with various electronic configurations on octahedral sites in fluoride crystals.[4,5] Other EPR measurements of transition ions in various crystals have been made.[6,7]

Although the EPR method has served as a powerful tool in various research problems, it frequently fails to make an unambiguous determination of the total defect structure. However, a more powerful technique than EPR is electron-nuclear double-resonance (ENDOR) introduced by Feher.[8] The high-precision determination of lattice hyperfine interactions by ENDOR permits a determination of the geometry of defects, impurities, and associations. Comparison of theoretical and experimental hyperfine interactions provides a picture of lattice distortion about the defect.[9-11]

Electron-nuclear double-resonance studies[10,11] of substitutional trivalent positive ions in CaF_2 have confirmed the existence of charge compensation by interstitial negative ions by direct observation of the ENDOR signals due to the nuclei of the interstitial ions. Since substitutional divalent positive ions in alkali halides are charge compensated by positive-ion vacancies, the ENDOR technique cannot provide the same direct demonstration of the charge compensator. The best data that an ENDOR study could obtain would be data for all possible lattice sites except the vacancy. Since no ENDOR signal can be obtained from a vacancy, its presence must still be inferred by the symmetry of the EPR and ENDOR data, and the behavior of the impurity when the crystal is subjected to radiation and various temperatures.

An ENDOR study of the Fe^+ ions in an octahedral site in NaF crystals (the octahedral center) was made by Chung and Mieher.[12] The octahedral centers consist of Fe^+ ions occupying the Na^+-ion sites substitutionally without any nearby association.

In this paper we report an ENDOR study of the Fe^+ center in an orthorhombic site in NaF crystal. The orthorhombic centers are produced by either electron bombardment or x-ray irradiation at liquid-helium temperature, and are stable up to about 60 K. Unfortunately, due to the large number of ENDOR lines resulting from the quadrupole splitting[12] of the Na ENDOR lines and the low symmetry of the associated complex, and due to the low frequencies of the Na ENDOR lines resulting from the large g values, we were unable to make a detailed ENDOR study of the Na nuclei, even though the Na nuclei were measured for the octahedral center.[12]

Garrison has made detailed EPR measurements of the orthorhombic center in x-ray irradiated NaF crystals.[13] The model suggested by Garrison is that Fe^+ ions in substitutional Na^+ sites are associated with a vacancy at the nearest Na^+ site (1, 1, 0). This vacancy was originally associated with the Fe^{2+} ion for charge compensation in the freshly grown crystal.[3-5] When the crystal is exposed to x rays at liquid-helium temperature, Fe^{2+} ions may trap an electron and become Fe^+ ions; however, the associated vacancy may not move at this low temperature, resulting in the orthorhombic centers. To confirm this model one needs to establish two things: one is the charge state and the other is the detailed structure of the surroundings. Garrison suggests that the charge state is Fe^+ based on the fact that this center

can be converted to the octahedral center (Fe^+) by warming, and that the g tensor has the value of $g_{xx}+g_{yy}+g_{zz}=10+3k$, with $k\simeq 0.8$, where the factor k represents the reduction of orbital angular momentum due to charge transfer, which is consistent with the theoretical value by Tinkham.[14] The determination by Garrison of the vacancy site was mainly based on the symmetry revealed by the g tensor, since it was not possible to determine accurate hyperfine constants for neighbor lattice nuclei in the EPR study. Our present ENDOR results are in agreement with the basic model. However, we shall show that the location of the vacancy with respect to the g tensor is different than that assigned by Garrison.

We have observed other evidence that is in favor of the Fe^+ state. The EPR spectrum has also been studied for an ultrapure NaF crystal, obtained from Cornell University, that was irradiated in the same manner as the Harshaw crystals. This sample was grown by a careful process of multiple zone refinings. From the investigation of the EPR spectrum, the Cornell sample was found to contain V_K centers in greatly reduced concentration (about 5%–10% of the V_K concentration in the Harsaw crystals), but H and F centers with about the same concentration as in the Harshaw crystals. Also, there was no sign of the Fe^+ resonance in the Cornell crystal. If one assumes that Fe^{2+} ions in the Harshaw crystals behave as electron traps, one may understand why the production of V_K centers is so much higher, and also that the production of other centers that do not require electron traps are about the same in the different samples. All of these details are in favor of the charge state of Fe^+ for both the octahedral and the orthorhombic centers.

Figure 1 shows a schematic diagram of the various structures and mechanisms of iron centers in NaF. This is a summary made from both the present and the previous studies.[4,5,12,13,15] Kim and associates have reported the EPR study of Fe^{3+} ions in NaF,[15,16] and the EPR result of Fe^{2+} ions in octahedral sites in NaF is given by Hall *et al.*[5] We observed complicated EPR spectra at liquid-helium temperature after the orthorhombic center was annealed to 60–250 °K, and the spectra were somewhat different for different annealing temperatures. These spectra were presumably due to Fe^+ centers associated with a vacancy at sites other than the nearest Na^+ site (1, 1, 0), i.e., the vacancy moved away, but not enough to leave the centers in an octahedral site. It has not yet been possible to analyze these spectra.

All the magnetic resonance data in this experiment were obtained on the X-band superheterodyne spectrometer described by Gazzinelli and Mieher,[17] operating at a signal frequency of 9370 MHz. The experimental procedure has been described in Ref. 12.

In this experiment we have used both the ⟨100⟩- and ⟨110⟩-rotation-axis samples to make the angular-dependence study in the {100} and {110} planes.

The ENDOR spectrum as a whole showed a dramatic temperature dependence. Over a 5 °K temperature range, ENDOR signals would vary in intensity by a factor of 50. Beyond the limits of this range, the signals were not visible. This characteristic of the spectrum presented many difficulties in initially obtaining the ENDOR resonances. Once the signals were obtained, the process of maximizing the signals with respect to temperature had to be repeated at each point in the angular dependence. The signals maximized in the range 9–14 °K. The temperature dependence of the ENDOR signals is illustrated by Fig. 2.

II. ENDOR RESULTS AND ANALYSIS

A. Preliminary

The environment of the orthorhombic center is shown in Fig. 3. We have analyzed the ENDOR spectrum of the neighboring fluorine nuclei in the first two shells. Each shell has three inequivalent sets of equivalent nuclei, which are labeled A, B, and C in the shell.

When the g tensor is strongly anisotropic, the electron spin is, in general, no longer quantized along the static field direction. The EPR line itself has a strong angular dependence, which in turn means that not only the orientation but also the magnitude of the laboratory magnetic field is changed as we rotate the crystal. However, there is still a reasonable way to analyze the ENDOR spectrum if we take the same sort of approximation as in Ref. 12, namely, if we assume that the electron spin $\vec{S}$ behaves according to the electron Zeeman term in the spin Hamiltonian,

$$\mathcal{H}=\mu_B\vec{H}_0\cdot\vec{\vec{g}}\cdot\vec{S}+\sum_j(-\mu_N g_j\vec{H}_0\cdot\vec{I}_j+\vec{I}_j\cdot\vec{\vec{A}}_j\cdot\vec{S}). \tag{1}$$

The assumption that $\vec{S}$ is quantized along $\vec{H}_0\cdot\vec{\vec{g}}$ is usually a good approximation, since $\mu_B H_0 g$ is much larger than A_j in most cases. Since we now have three different coordinate systems (the principal-axes system of the g tensor, that of the A tensor, and the crystal axes), it is rather complicated to have a general formula. Therefore, in the following sections we shall consider one particular case at a time.

Before proceeding to Sec. IIB, we should first

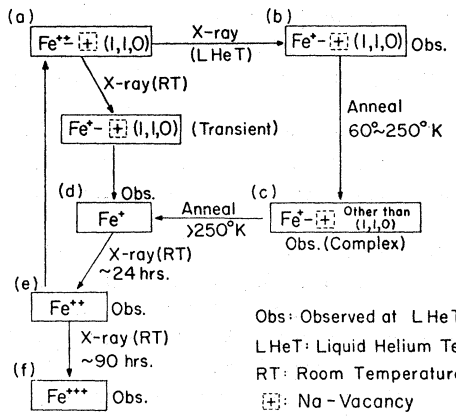

FIG. 1. Schematic diagram of the various possible structures of iron centers in NaF. (a) In a fresh NaF crystal Fe^{2+} substitutes for Na^+ and charge is compensated with a Na^+ vacancy at (1,1,0) site. (b) When x-rayed at liquid-helium temperature Fe^{2+} changes its charge state to Fe^+, but the vacancy stays at (1,1,0). (c) When the state *B* was annealed to 60–250 K, the Na vacancy moved to other sites than (1,1,0), resulting in complex EPR lines. (d) When the state *C* was annealed further to above 250 K, the vacancy moved away enough to leave Fe^+ in octahedral site. On the other hand, this state can also be obtained by x-irradiation of the state *A* at room temperature (RT). (e) When the state *D* is x-rayed longer (~ 24 h) at RT, Fe^+ changes its charge state to Fe^{2+}. When this state *E* is left at RT without irradiating, it goes back to the original state *A* (see Refs. 4 and 5). (f) When the state *E* is further x-rayed (~ 90 h) at RT, Fe^{2+} changes to Fe^{3+} (Ref. 16).

give a preliminary account of the EPR measurements, since this is needed to understand the details of the ENDOR spectrum. Since this paramagnetic impurity does not have a nuclear magnetic moment (only the 2%-abundant isotope ^{57}Fe has a nuclear magnetic moment), from Eq. (1) the resonant field for the EPR line may be given by

$$H_0 = h\nu_e/\mu_B g' . \tag{2}$$

In the above equation, ν_e is the EPR frequency and

$$g' \equiv (g_x^2\cos^2\alpha + g_y^2\cos^2\beta + g_z^2\cos^2\gamma)^{1/2},$$

where $\cos\alpha$, $\cos\beta$, and $\cos\gamma$, are the direction cosines of $\vec{H}_0$ in the g-tensor principal-axes system. So if we know the g tensor and its principal axes, then we can easily find its angular dependence by simply expressing $\cos\alpha$, $\cos\beta$, and $\cos\gamma$ in terms of the rotation angle θ. In practice, the g tensor is found from the experimental angular dependence of the EPR spectra. The g tensor of this orthorhombic center is $g_x = 2.027 \pm 0.002$, $g_y = 5.797 \pm 0.002$, and $g_z = 4.588 \pm 0.002$ with a set of corresponding axes parallel to $[00\bar{1}]$, $[1\bar{1}0]$, and [110], respectively. This in close agreement with the values of Ref. 13, where $g_x = 2.029 \pm 0.002$, $g_y = 5.792 \pm 0.002$, and $g_z = 4.585 \pm 0.002$.

For a general orientation of the magnetic field, we shall have six EPR lines at magnetic fields given by Eq. (2), since there are six possible

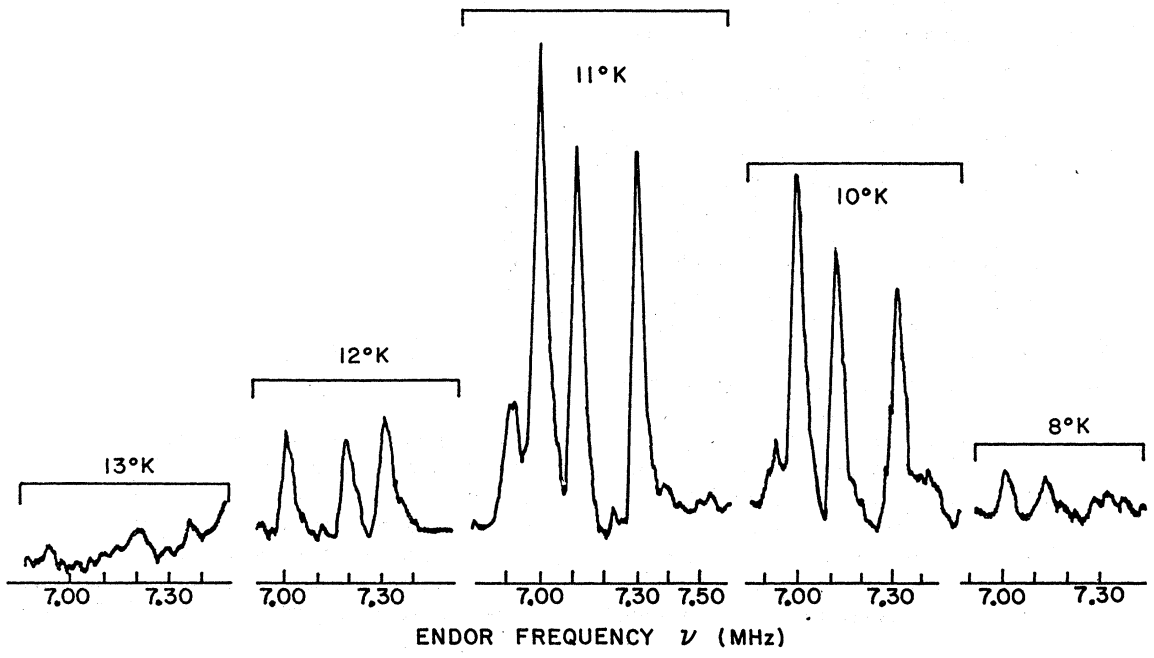

FIG. 2. Temperature dependence of the fluorine ENDOR spectrum.

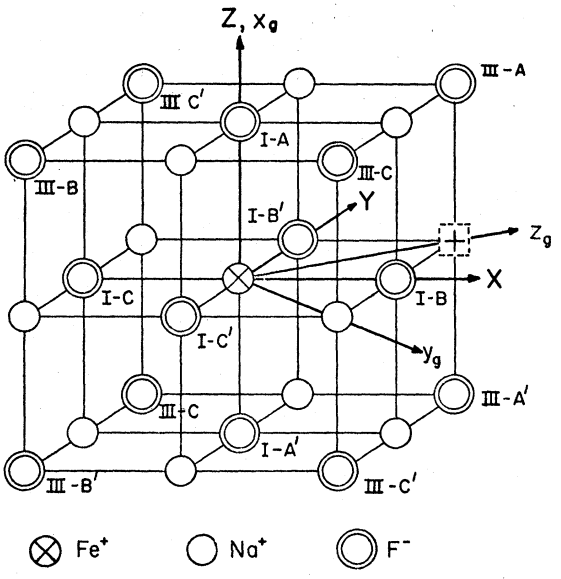

FIG. 3. Lattice near the orthorhombic center.

orientations of the principal axes of this g tensor as given in Table I. One of these systems [(a) in Table I] is shown in Fig. 3, where the spatial coordinates X, Y, and Z fixed in the crystal are also shown.

Suppose that the Z-X plane in Fig. 3 is the plane of rotation of $\vec{H}_0$ (in the case of the $\langle 100\rangle$-rotation-axis sample) and that we measure the rotation angle θ from the Z axis ([001]), then the static field may be written

$$\vec{H}_0 = H_0 \hat{H}_0 = H_0(\sin\theta,\ 0,\ \cos\theta),$$

where we have used the notation

$$(A,B,C) \equiv A\hat{x} + B\hat{y} + C\hat{z},$$

and we can find

$$\cos\alpha = \hat{H}_0 \cdot \hat{x}_g, \quad \cos\beta = \hat{H}_0 \cdot \hat{y}_g, \quad \cos\gamma = \hat{H}_0 \cdot \hat{z}_g. \quad (3)$$

From Table I and Eq. (3), we can find all six EPR lines given by Eq. (2), but we immediately find that EPR lines from (a) and (b) are the same, and so are (e) and (f). Therefore, when $\hat{H}_0$ is in the Z-X plane, we have four EPR lines, and, for example, the EPR line of (a) can be written

$$H_0 = h\nu_e/\mu_B(g_x^2\cos^2\theta + \tfrac{1}{2}g_y^2\sin^2\theta + \tfrac{1}{2}g_z^2\sin^2\theta)^{1/2}, \quad (4)$$

and we will have similar expressions for the other lines. Figure 4 shows the angular dependence of the four EPR lines. In this figure, the line with crosses is the EPR line given by Eq. (4), along which the ENDOR measurements have been made with the $\langle 100\rangle$ sample.

Now, consider the situation of the $\langle 110\rangle$-rotation-axis sample. In this case we rotate $\vec{H}_0$ from [001] to [110] in the $(1\bar{1}0)$ plane; hence the static field can be written

$$\vec{H}_0 = H_0\hat{H}_0 = H_0(\sin\theta/\sqrt{2},\ \sin\theta/\sqrt{2},\ \cos\theta). \quad (5)$$

Again using Eq. (3) with Table I and Eq. (5), we can find the direction cosines, which in turn will give six EPR lines by Eq. (2). However, the EPR lines from (c) and (e) are the same, and so are (d) and (f), and consequently we have only four lines. The equation for the EPR line of (a) in Table I can be written

$$H_0 = h\nu_e/\mu_B(g_x^2\cos^2\theta + g_z^2\sin^2\theta)^{1/2}, \quad (6)$$

which we will call EPR line 2, and for the EPR line of (b) one can write

$$H_0 = h\nu_e/\mu_B(g_x^2\cos^2\theta + g_y^2\sin^2\theta)^{1/2}, \quad (7)$$

which we will call EPR line 1.

Figure 5 shows the angular dependence of all four EPR lines, along with the observed values. In this figure the triangles are the observed values

TABLE I. Six possible sets of the g-tensor principal-axes systems of the orthohombic center in the spatial X, Y, Z coordinates in Fig. 3.

Set	Directions of the principal axes			Unit vectors of the principal axes in the X, Y, Z, system		
	x_g	y_g	z_g	$\hat{x}_g$	$\hat{y}_g$	$\hat{z}_g$
(a)	[001]	$[1\bar{1}0]$	[110]	(0, 0, 1)	$(1, -1, 0)/\sqrt{2}$	$(1, 1, 0)/\sqrt{2}$
(b)	$[00\bar{1}]$	[110]	$[1\bar{1}0]$	(0, 0, -1)	$(1, 1, 0)/\sqrt{2}$	$(1, -1, 0)/\sqrt{2}$
(c)	[010]	[101]	$[10\bar{1}]$	(0, 1, 0)	$(1, 0, 1)/\sqrt{2}$	$(1, 0, -1)/\sqrt{2}$
(d)	$[0\bar{1}0]$	$[10\bar{1}]$	[101]	(0, -1, 0)	$(1, 0, -1)/\sqrt{2}$	$(1, 0, 1)/\sqrt{2}$
(e)	[100]	[011]	$[0\bar{1}1]$	(1, 0, 0)	$(0, 1, 1)/\sqrt{2}$	$(0, -1, 1)/\sqrt{2}$
(f)	$[\bar{1}00]$	$[0\bar{1}1]$	[011]	(-1, 0, 0)	$(0, -1, 1)/\sqrt{2}$	$(0, 1, 1)/\sqrt{2}$

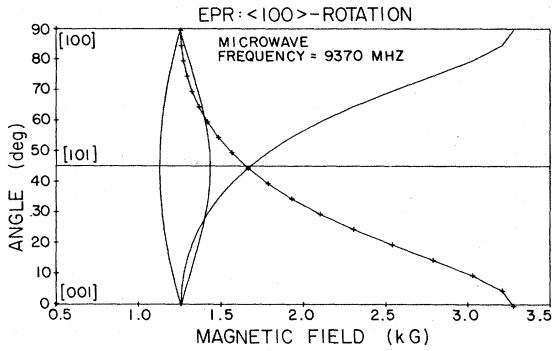

FIG. 4. Angular dependence of the calculated EPR of the orthorhombic center with the ⟨100⟩ sample. ENDOR measurements have been taken on the line with crosses.

along the EPR line 1 and the circles are the observed values along the EPR line 2.

When we derived Eq. (7), we took the different set of the principal axes of the g tensor with the plane of rotation of $\vec{H}_0$ fixed [i.e., the $(1\bar{1}0)$ plane]; however, this is physically the same as changing the plane of rotation of $\vec{H}_0$ to the (110) plane (x_g-y_g plane). In other words, when we follow the EPR line 1 the static field is in the x_g-y_g plane, and when we follow the EPR line 2 the field is in the x_g-z_g plane. All the ENDOR measurements with the ⟨110⟩ sample have been made along these two EPR lines. This will make it somewhat simpler to analyze the ENDOR results, since the spin $\vec{S}$ will remain in one of the principal planes of the g tensor (which are also the rotation planes of $\vec{H}_0$). This is, however, not the case for the ⟨100⟩ sample. For the ⟨100⟩ sample $\vec{S}$ will not be in the rotation plane of $\vec{H}_0$, since the rotation plane is not a principal plane of the g tensor.

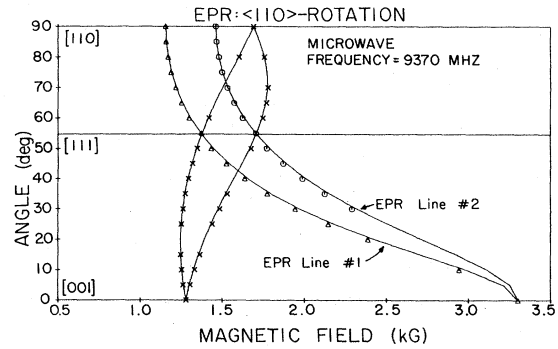

FIG. 5. Angular dependence of the calculated EPR of the orthorhombic center with the ⟨110⟩ sample.

B. Shells I-*A*, I-*B*, and I-*C*

Assuming that we already know the model as shown in Fig. 3, we shall start with the nuclei I-A and I-A'. The ENDOR data of these two nuclei have been taken along the EPR lines 1 and 2. Since for these two EPR lines the magnetic field lies in the g-tensor principal planes, as shown in Sec. II A, we shall work in the g-tensor axes system. Accordingly, all the necessary quantities should be properly expressed in these g-tensor coordinates. Since the z_g-x_g plane is the plane of reflection symmetry of I-A and I-A', as can be seen in Fig. 3, one of the principal axes of the hyperfine tensor of this nucleus should be perpendicular to this plane, and we shall call this the y axis. Consequently, the other two hyperfine axes (z axis and x axis) should lie in the z_g-x_g plane, and let ϕ be the angle between the z axis and the x_g axis, as shown in Fig. 6(a). Then, the unit vectors of the hyperfine x,y,x axes in the x_g, y_g, z_g coordinates become

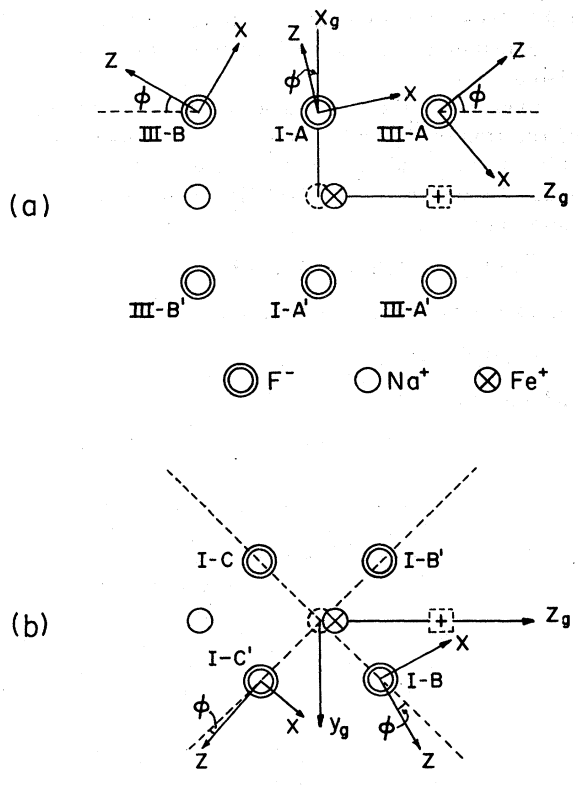

FIG. 6. Hyperfine principal axes. (a) The principal axes of I-A, III-A, and III-B. (b) The principal axes of the I-B and I-C. The φ's are different for B and C.

$$\hat{x} = (\sin\phi,\ 0,\ \cos\phi),$$
$$\hat{y} = (0,\ -1,\ 0), \tag{8}$$
$$\hat{z} = (\cos\phi,\ 0,\ -\sin\phi),$$

where we have used the notation $(A,B,C) \equiv A\hat{x}_g + B\hat{y}_g + C\hat{z}_g$.

First, consider the ENDOR along the EPR 2 (see Fig. 5). From Eq. (6) we note that the electron spin $\vec{S}$ sees the effective static field,

$$\vec{H}_{\text{eff}} = H_0(g_x\cos\theta,\ 0,\ g_z\sin\theta) = H_0 g(\theta)(g_x\cos\theta,\ 0,\ g_z\sin\theta)/g(\theta),$$

where

$$g(\theta) \equiv (g_x^2\cos^2\theta + g_z^2\sin^2\theta)^{1/2}. \tag{9}$$

Or, we may as well say that $\vec{S}$ is quantized along the direction

$$\hat{S} \equiv (g_x\cos\theta,\ 0,\ g_z\sin\theta)/g(\theta), \tag{10}$$
$$\equiv (\cos\psi,\ 0,\ \sin\psi),$$

where we have defined

$$\cos\psi = g_x\cos\theta/g(\theta) \quad \text{and} \quad \sin\psi = g_z\sin\theta/g(\theta);$$

then, ψ is the angle between $\vec{S}$ and the x_g axis. All of these angular relations are shown in Fig. 7.

If we go through the arguments given in Ref. 12, then we can write the effective field at the nucleus I-A as

$$\begin{aligned} H_x &= (m_s A_x \hat{x}\cdot\hat{S} - \gamma_F\hbar H_0\hat{x}\cdot\hat{H}_0)/\gamma_F\hbar, \\ H_y &= (m_s A_y \hat{y}\cdot\hat{S} - \gamma_F\hbar H_0\hat{y}\cdot\hat{H}_0)/\gamma_F\hbar, \\ H_z &= (m_s A_z \hat{z}\cdot\hat{S} - \gamma_F\hbar H_0\hat{z}\cdot\hat{H}_0)/\gamma_F\hbar, \end{aligned} \tag{11}$$

where H_x is the x component of the effective field in the hyperfine axes system of I-A, etc., and

$$\hat{H}_0 = (\cos\theta,\ 0,\ \sin\theta). \tag{12}$$

From Eq. (11), with Eqs. (8) and (10) we can write the ENDOR frequency ν of I-A as

$$\begin{aligned} h\nu = \{&[m_s A_x(g_x\sin\phi\cos\theta + g_z\cos\phi\sin\theta)/g(\theta) \\ &-\gamma_F\hbar H_0(\sin\phi\cos\theta + \cos\phi\sin\theta)]^2 \\ &+[m_s A_z(g_x\cos\phi\cos\theta - g_z\sin\phi\sin\theta)/g(\theta) \\ &-\gamma_F\hbar H_0(\cos\phi\cos\theta - \sin\phi\sin\theta)]^2\}^{1/2}, \end{aligned} \tag{13}$$

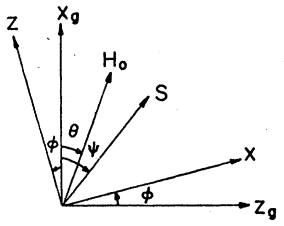

FIG. 7. Angular relations of $\vec{H}_0$, $\vec{S}$, and the hyperfine axes in the g-tensor principal-axes system.

with $g(\theta)$ given by Eq. (9) and

$$H_0 = h\nu_e/g(\theta)\mu_B.$$

Thus an expression of the ENDOR frequency of the nucleus I-A has been found as a function of the rotation angle θ, with the parameters A_z, A_x, and ϕ to be determined.

The ENDOR frequency of the nucleus I-A' can be found by changing the sign of θ in Eq. (13), because to the nucleus I-A' the above magnetic field seems to rotate to the opposite direction [see Fig 8(a)]. Thus for the nucleus I-A', we have

$$h\nu' = h\nu(-\theta) \tag{14}$$

of Eq. (13).

Therefore, we will observe two ENDOR lines from I-A and I-A' by Eqs. (13) and (14) for each m_s, except for $\theta = 0°$ (i.e, along [001]) and $\theta = 90°$ (along [110]), in which cases the two ENDOR lines coincide.

A nonlinear least-squares-fitting computer proggram (NONLINR) has been used to fit the observed ENDOR data to Eqs. (13) and (14) to determine A_z, A_x, and ϕ, which are given in Table II. Figure 8 shows the computer plot of the calculated and observed angular dependence of the ENDOR spectra of the nuclei I-A and I-A'; the circles are the observed ENDOR values for the EPR 2.

Similarly, we can find the ENDOR frequency of the nucleus I-A along the EPR 1 as

$$\begin{aligned} h\nu = \{&[m_s A_x g_x\sin\phi\cos\theta/g(\theta) - \gamma_F\hbar H_0\sin\phi\cos\theta]^2 \\ &+[m_s A_y g_y\sin\theta/g(\theta) - \gamma_F\hbar H_0\sin\theta]^2 \\ &+[m_s A_z g_z\cos\phi\cos\theta/g(\theta) \\ &-\gamma_F\hbar H_0\cos\phi\cos\theta]^2\}^{1/2}, \end{aligned} \tag{15}$$

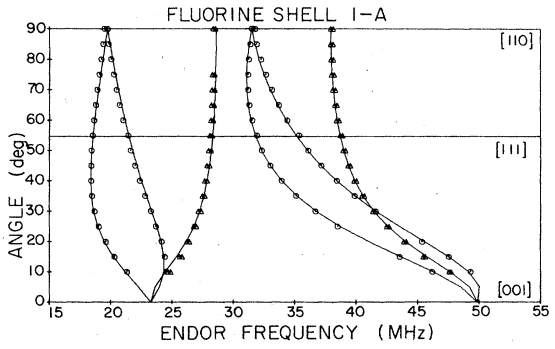

FIG. 8. Angular dependence of the calculated and observed ENDOR of I-A. The triangles are the observed ENDOR values along the EPR line 1 and the circles along line 2.

TABLE II. Hyperfine constants of the nuclei I-A for the orthorhombic center. The principal axes are defined in Fig. 6(a).

	Present work	Previous EPR[a]
ϕ	11.8° ± 0.2°	0
A_z	74.0 ± 0.1 (MHz)	74.2 ± 2.0 (MHz)
A_x	50.0 ± 0.05 (MHz)	47.0 ± 3.0 (MHz)
A_y	66.5 ± 0.1 (MHz)	69.0 ± 5.0 (MHz)

[a] See Ref. 13. The value of ϕ is not given by Garrison. However, the principal axes chosen there implies this value.

where

$$g(\theta) = (g_x^2 \cos^2\theta + g_y^2 \sin^2\theta)^{1/2} \tag{16}$$

and

$$H_0(\theta) = h\nu_e / g(\theta)\mu_B .$$

To find the similar expression for the nucleus I-A' (see Fig. 3), we can simply substitute $\theta = \theta + 180°$ in Eq. (15), which in turn gives us the same equation as Eq. (15). In other words, when we follow the EPR Line 1, the nuclei I-A and I-A' will give rise to a single ENDOR line for each m_s; hence we will observe two lines approximately $2\gamma_F \hbar H_0$ apart given by Eq. (15). When $\theta = 90°$, Eq. (15) becomes

$$h\nu(90°) = \tfrac{1}{2}A_y \pm \gamma_F \hbar H_0 . \tag{17}$$

From this equation we can find A_y by the ENDOR data with $\theta = 90°$ along the EPR line 1, because the static field is along the hyperfine y axis (i.e., the hyperfine y axis coincides the y_g axis).

Table II gives A_y along with the previously determined A_z, A_x, and ϕ. This table also gives the values determined by Garrison in his EPR study for comparison.

Figure 8 also shows the calculated and observed ENDOR spectra for I-A and I-A' along the EPR line 1. In this figure the solid line is the calculated angular dependence using Eq. (15) with the parameters given in Table II, and the triangles are the observed values. The observed ENDOR spectrum shows a doublet structure, which is due to the higher-order effects of the two equivalent nuclei.[7,12]

Next, let us consider the four remaining nuclei in shell I, namely, I-B, I-B', I-C, and I-C' in the (001) plane (see Fig. 3). Since the (001) plane is the plane of the reflection symmetry for these nuclei, one of the principal axes should be perpendicular to this plane, i.e., parallel to the [001] direction, and accordingly the other two should lie in the (001) plane. The presence of a vacancy makes I-B and I-C inequivalent. So, we shall assume that the hyperfine z axis of I-B makes an angle ϕ with the [100] direction and that of I-C makes ϕ with the $[\bar{1}00]$ direction, as shown in Fig. 6(b) (the ϕ's are different for B and C).

For these nuclei we have made the ENDOR measurements with the magnetic field in the (010), $(1\bar{1}0)$, and (110) planes, which correspond to the EPR lines of Eqs. (4), (6), and (7), respectively.

Along the EPR line of Eq. (4) [the EPR line with crosses on it (Fig. (4)], we can find the ENDOR frequency of I-B as

$$h\nu = \{\{m_s A_x [\tfrac{1}{2}(g_z + g_y)\sin\phi\sin\theta + \tfrac{1}{2}(g_z - g_y)\cos\phi\sin\theta]/g(\theta) - \gamma_F \hbar H_0 \sin\phi\sin\theta\}^2 + [m_s A_y g_x \cos\theta/g(\theta) - \gamma_F \hbar H_0 \cos\theta]^2 + \{m_s A_z [\tfrac{1}{2}(g_z + g_y)\cos\phi\sin\theta - \tfrac{1}{2}(g_z - g_y)\sin\phi\sin\theta]/g(\theta) - \gamma_F \hbar H_0 \cos\phi\sin\theta\}^2\}^{1/2}, \tag{18}$$

where

$$g(\theta) = (g_x^2\cos^2\theta + \tfrac{1}{2}g_y^2\sin^2\theta + \tfrac{1}{2}g_z^2\sin^2\theta)^{1/2},$$

and

$$H_0 = H_0(\theta) = h\nu_e / \mu_B g(\theta) .$$

Although this expression is complicated, it is a function of only θ, the rotation angle of the static field, with the parameters A_x, A_y, A_z, and ϕ. The complication comes from the fact that the magnetic field is in a general orientation to both g- and A-tensor principal-axes system. Similarly, we can find the ENDOR frequencies for I-B', I-C, and I-C'.

When the static field is in the $(1\bar{1}0)$ plane (the EPR line 2) or in the (110) plane (the EPR line 1), all the nuclei I-B, I-B', I-C, and I-C$'$ will have the same expression of the ENDOR frequency. For the EPR line 2, we obtain for the nucleus I-B

$$h\nu = \{[m_s A_x g_z \sin(45° + \phi)\sin\theta/g(\theta) - \gamma_F \hbar H_0 \sin(45° + \phi)\sin\theta]^2 + [m_s A_y g_x \cos\theta/g(\theta) - \gamma_F \hbar H_0 \cos\theta]^2 + [m_s A_z g_z \sin(45° - \phi)\sin\theta/g(\theta) - \gamma_F \hbar H_0 \sin(45° - \phi)\sin\theta]^2\}^{1/2}, \tag{19}$$

with $g(\theta)$ given by Eq. (9) and $H_0 = h\nu_e/g(\theta)\mu_B$.

Similarly, for the EPR line 1, we obtain for nucleus I-B

$$h\nu = \{[m_s A_x g_y \cos(45°+\phi)\sin\theta/g(\theta) - \gamma_F \hbar H_0 \cos(45°+\phi)\sin\theta]^2 + [m_s A_y g_x \cos\theta/g(\theta) - \gamma_F \hbar H_0 \cos\theta]^2 + [m_s A_z g_y \cos(45°-\phi)\sin\theta/g(\theta) - \gamma_F \hbar H_0 \cos(45°-\phi)\sin\theta]^2\}^{1/2}, \quad (20)$$

with $g(\theta)$ given by Eq. (16) and $H_0 = h\nu_e/g(\theta)\mu_B$.

Considerations of symmetry show that I-B and I-B' have the same parameters, and likewise I-C and I-C'. The actual ENDOR spectrum has a complex multiplet structure due to the higher-order interactions discussed in detail for the octahedral center in Ref. 12, and the structure strongly depends on the orientation. Therefore, in the fitting process we have taken the center of the multiplet structure. All the ENDOR data for these nuclei have been fit by NONLINR to Eqs. (18)–(20) to determine the hyperfine constants. Table III gives the parameters thus determined.

Figure 9 shows the angular dependence of the ENDOR of the four nuclei with the parameters in Table III when the static field is in the (010) plane. In this figure the circles are the observed values for I-B and I-B', and the triangles are those for I-C and I-C'. These values are the center frequencies of the complex multiplet as mentioned above. Figure 10 shows the angular dependence of the ENDOR spectrum when the static field is in the (110) plane (i.e., along the EPR line 1). The crosses are the observed values or I-C', and the ×'s are those for I-B and I-B'. Figure 11 shows the angular dependence of the ENDOR spectrum when the static field is in the (1$\bar{1}$0) plane (i.e., along the EPR line 2). The crosses in the figure are the observed values for I-C and I-C'.

TABLE III. Hyperfine constants of the nuclei I-B and I-C for the orthorhombic center. The principal axes are defined in Fig. 6(b).

Shell	Present work I-B	Present work I-C	Previous EPR[a] I-B and I-C
ϕ (degrees)	15.9 ± 3.0	4.5 ± 2.0	5.6
A_z (MHz)	157.0 ± 3.0	133.7 ± 2.0	134.6
A_x (MHz)	43.1 ± 5.0	49.6 ± 2	62.3
A_y (MHz)	26.9 ± 0.2	26.9 ± 0.2	26.8

[a] See Ref. 13. Values were given in tensor-component form in the g-tensor coordinate system as follows: $A_{xx} = 85.6 \pm 3$, $A_{yy} = 26.8 \pm 2$, $A_{zz} = 111.3 \pm 3$, $A_{xx} = 33.8 \pm 3$. We have diagonalized them for comparison.

C. Shells III-A, III-B, and III-C

The ENDOR spectra around $\gamma_F H_0$ have been measured within about 30° of the [110] direction for EPR Line No. 2 and of the [1$\bar{1}$0] direction for EPR line 1, and they have been identified as those from the nuclei III-A, III-B, and III-C (see Fig. 3). Electron-nuclear double-resonance lines from some of the shell-V-type nuclei (2, 1, 0) were observed, but the hyperfine constants were not determined due to insufficient data.

The III-A sites lie in the z_g-x_g plane, which is a plane of reflection symmetry. As shown in Fig. 6(a), the situation is similar to that of I-A nucleus. Therefore, the mathematical formalism is essentially the same as the one given for I-A, and we can obtain the ENDOR expression along the EPR line 2 by a simple substitution of ϕ by $\phi - 90°$ and θ by $90° - \theta$ in Eq. (13). Now, θ is measured from the [110] direction to the [001] direction and is the angle defined in Fig. 6(a). Thus we obtain

$$h\nu = \{[m_s A_x(-g_x \cos\phi \sin\theta + g_z \sin\phi \cos\theta)/g(\theta) - \gamma_F \hbar H_0(-\cos\phi \sin\theta + \sin\phi \cos\theta)]^2 + [m_s A_z(g_x \sin\phi \sin\theta + g_z \cos\phi \cos\theta)/g(\theta) - \gamma_F \hbar H_0(\sin\phi \sin\theta + \cos\phi \cos\theta)]^2\}^{1/2}, \quad (21)$$

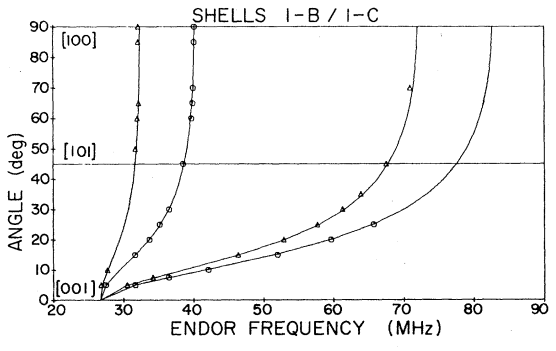

FIG. 9. Angular dependence of the calculated and observed ENDOR of I-B and I-C along the EPR line of Fig. 4. The circles are the center frequencies of the observed values for I-B, and the triangles are those for I-C.

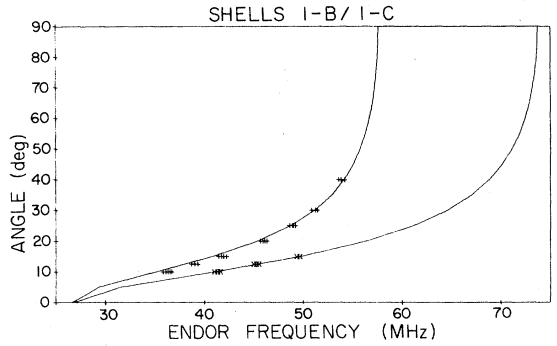

FIG. 10. Angular dependence of the calculated and observed ENDOR of I-B and I-C along the EPR line 1 in Fig. 5, i.e., when the static field is in the (110) plane. The crosses are the observed values for I-C, and X's are those for I-B.

where

$$g(\theta) = (g_x^2 \sin^2\theta + g_z^2 \cos^2\theta)^{1/2}$$

and

$$H_0 = H_0(\theta) = h\nu_e/\mu_B g(\theta) .$$

For III-A' we obtain a similar expression by substituting $-\theta$ into θ in Eq. (21). The ENDOR measurements have been fit to Eq. (21) by using the NONLINR program, and the parameters thus determined are given in Table IV. A_y has been determined from the ENDOR of the EPR line 1 with Eq. (17).

As shown in Fig. 6(a), the equivalency of III-A and III-B is broken by the presence of a vacancy. Since the nature of the local symmetry is the same for these two shells, the expressions for the ENDOR frequencies are identical with, of course, slightly different values of parameters. Therefore, a doublelike ENDOR spectra is to be expected. This doublet, however, is fundamentally different from the one observed for I-A. The former is due to the slight inequivalency of the two nuclei, while the latter is due to the higher-order effects for two equivalent nuclei.

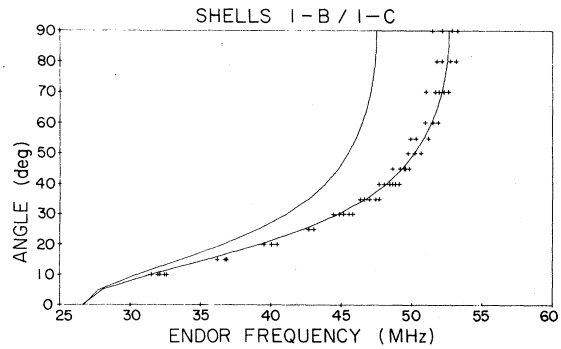

FIG. 11. Angular dependence of the calculated and observed ENDOR of I-B and I-C along the EPR line 2 in Fig. 5, i.e., when the static field is in the (1$\bar{1}$0) plane. The crosses are the observed values for I-C.

It should be pointed out that the assignment of the experimental lines labeled III-A and III-B to their corresponding sites in Fig. 6(a) is based primarily on considerations of the experimental angles ϕ listed in Table IV. Assuming the Fe^+ ion to relax toward the vacancy, we have simply assigned the nuclei so that the hyperfine z axis may be close to the direction of $Fe^+ - F^-$. The same considerations have been used in the assignments of I-B and I-C in Fig. 6(b).

Figure 12 shows the calculated and observed angular dependence of the ENDOR spectrum of III-A and III-B along the EPR line 2. In this figure the circles are the measured values of III-A, and the triangles are those of III-B.

Finally, let us look at the nucleus III-C. As we see in Fig. 3, this does not have any local symmetry at all. Therefore, none of the hyperfine axes can be determined by symmetry considerations. Furthermore, we do not have enough data to experimentally determine those axes. Therefore, we made a crude assumption. Namely, since one of the hyperfine planes may not deviate much from the x_g-y_g plane, we have assumed that one hyperfine plane coincides with the x_g-y_g plane. Then the situation becomes the same as that of III-A, and we can use the same equations derived for III-A. Since we are now with the EPR line 1, the g values should be properly replaced in Eqs. (21) and (22). It should be noted that when the static field is in the x_g-y_g plane, the two nuclei labeled by III-C are equivalent, and so are the two III-C' nuclei (Fig. 3), even though the hyperfine plane does not coincide with the x_g-y_g plane. Figure 13 shows the calculated and observed angular dependence of III-C, using a similar equation as Eq. (21) with the parameters given in

TABLE IV. Hyperfine constants of the nuclei III-A, III-B, and III-C for the orthorhombic center. The principal axes are defined in Fig. 6(a).

	III-A	III-B	III-C
ϕ (degrees)	33.8 ± 0.5	30.7 ± 0.5	30.4 ± 0.4
A_z (MHz)	3.69 ± 0.03	3.66 ± 0.04	5.22 ± 0.03
A_x (MHz)	-2.46 ± 0.08	-2.40 ± 0.09	-3.00 ± 0.12
A_y (MHz)	-3.25 ± 0.02	-3.53 ± 0.02	-2.90 ± 0.02

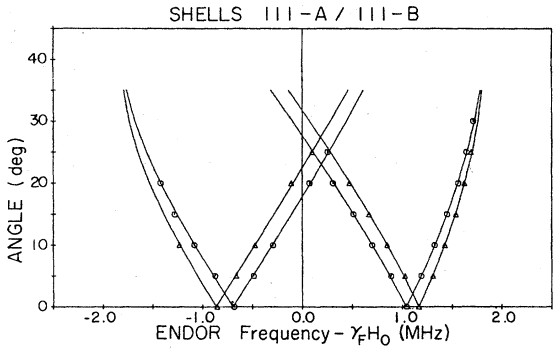

FIG. 12. Angular dependence of the calculated and observed ENDOR of III-*A* (circles) and III-*B* (triangles) along the EPR line 2 near the [110] direction.

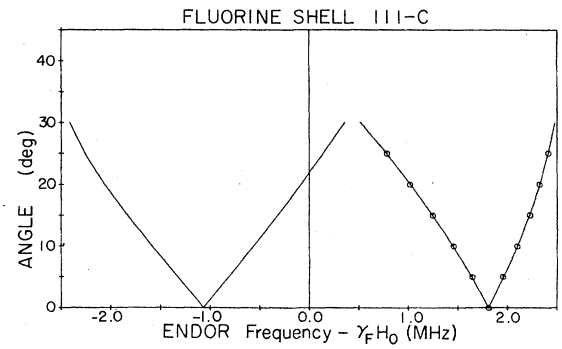

FIG. 13. Angular dependence of the calculated and observed ENDOR of III-*C* along the EPR line 1 near the [1$\bar{1}$0] direction.

Table IV. It is interesting to note that the hyperfine values in Table IV are very similar for nuclei III-*A* and III-*B*, and the values for III-*C* are quite different. The III-*A* and III-*B* nuclei are nonequivalent due to the presence of the vacancy, but are equivalent with respect to the g tensor axes, whereas the III-*C* nuclei are nonequivalent to III-*A* and III-*B* due to the vacancy and, also, due to a different location with respect to the g-tensor axes.

III. CONCLUSIONS AND DISCUSSIONS

We have determined the hyperfine tensors of the nearest-neighbor flurorine nuclei (shell I) of the orthorhombic center. Here we have clearly distinguished three inequivalent sets (labeled I-*A*, I-*B*, and I-*C*) of two equivalent nuclei. From these and the additional ENDOR measurements for the next-nearest-neighbor fluorine nuclei (III-*A*, III-*B*, and III-*C*), we have confirmed the basic idea of the model of this center suggested by Garrison based on his EPR study.[13] Namely, Fe^+ ions substitutionally occupying the Na^+ sites are associated with the nearest Na^+ vacancy in one of the ⟨110⟩ directions. The model of the vacancy association was mainly based on the symmetry of the g tensor (the principal values are $g_x = 2.027$, $g_y = 5.797$, $g_z = 4.588$, with [001], [1$\bar{1}$0], [110] axes as their respective principal axis), which requires something along either the [1$\bar{1}$0] direction or the [110] direction to give this symmetry. The previous assignment[13] of the vacancy position along the [1$\bar{1}$0] direction (associated with $g_y = 5.797$), however, was highly speculative since the accurate determination of the hyperfine tensors of the three distinct sets of the nearest neighbors was not possible with the EPR measurements. As we have seen in Sec. II, the hyperfine tensor of I-*A* nuclei determined by ENDOR tells us that the vacancy position should be along the [110] direction (associated with $g_z = 4.588$), which is different from Garrison's assignment. The additional ENDOR measurements for III-*A*, III-*B*, and III-*C* lattice nuclei also support this assignment of the vacancy site.

ACKNOWLEDGMENTS

This work was supported by the NSF under Grant No. DMR 73-02648. We wish to thank Professor J. W. MacKay, Purdue University, and his staff for the opportunity to use their 4.5-MeV electron linear accelerator. We also wish to thank Professor R. O. Pohl, Cornell University, for providing the sample of ultrapure NaF.

*Present address: Korea Standards Research Institute, Dae Duk, Korea.
†Present address: Varian, Radiation Division, Plymouth, Michigan 48170.

[1]F. Seitz, Rev. Mod. Phys. 26, 7 (1954).
[2]G. D. Watkins, Phys. Rev. 113, 79 (1959).
[3]W. Hayes, J. Appl. Phys. Suppl. 33, 329 (1962).
[4]T. P. P. Hall, W. Hayes, R. W. H. Stevenson, and J. Wilkins, J. Chem. Phys. 38, 1977 (1963).
[5]T. P. P. Hall, W. Hayes, R. W. H. Stevenson, and J. Wilkens, J. Chem. Phys. 39, 35 (1963).
[6]J. W. Orton, *Electron Paramagnetic Resonance* (Gordon and Breach, New York, 1968).
[7]A. Abragam and B. Bleaney, *Electron Paramagnetic Resonance of Transition Ions* (Clarendon, Oxford, 1970).

[8]G. Feher, Phys. Rev. 103, 834 (1956).
[9]D. F. Daly and R. L. Mieher, Phys. Rev. 175, 412 (1968).
[10]J. M. Baker, E. R. Davies, and T. R. Reddy, Contemp. Phys. 13, 45 (1972).
[11]J. M. Baker, E. R. Davies, and J. P. Hurrell, Phys. Lett. A 26, 352 (1968); Proc. R. Soc. A 308, 403 (1968).
[12]N. S. Chung and R. L. Mieher, Phys. Rev. B 12, 4755 (1975).
[13]A. K. Garrison, Mater. Res. Bull. 2, 155 (1967).
[14]M. Tinkham, Proc. R. Soc. A 236, 549 (1956).
[15]R. A. Andrew, and Y. M. Kim, Phys. Rev. 154, 220 (1967).
[16]H. L. Van Camp and Y. W. Kim, Phys. Rev. B 11, 3098 (1975).
[17]R. Gazzinelli and R. L. Mieher, Phys. Rev. 175, 395 (1968).